Pattern Recognition 65 (2017) 296–306

Contents lists available at ScienceDirect

Pattern Recognition

journal homepage: www.elsevier.com/locate/pr

Sparse 3D directional vertices vs continuous 3D curves: Efficient 3D surface matching and its application for single model face recognition

Xun Yu[a], Yongsheng Gao[a,*], Jun Zhou[b]

[a] School of Engineering, Griffith University, QLD 4111, Australia
[b] School of Information and Communication Technology, Griffith University, QLD 4111, Australia

ARTICLE INFO

Keywords:
3D surface matching
3D directional vertex
Fast 3D matching
Storage space
3D face recognition
3D curve
Hausdorff distance
Iterative closest points

ABSTRACT

Traditionally, point clouds and meshes are used to represent and match 3D shapes, which often cannot meet the computational speed and storage space requirements in many 3D data matching and retrieval applications. In this paper, we present a novel 3D directional vertices ($3D^2V$) approach to efficiently represent and match 3D surfaces by much fewer sparsely distributed structured vertices that carry structural information transferred from their deleted neighbouring points. A $3D^2V$ conversion and similarity measurement method is developed to compute the distance between two different $3D^2Vs$. The performance of the proposed method is evaluated on 3D face recognition using Face Recognition Grand Challenge v2.0 (FRGC v2.0) and GavabDB databases and compared with the curve-based benchmark method. The experimental results demonstrate that the proposed $3D^2V$ method can significantly reduce the data storage requirement and computation time with a moderate increase of accuracy at the same time. It provides a new tool for developing fast 3D surface matching algorithms for large scale 3D data classification and retrieval.

1. Introduction

Using 3D information for object recognition has attracted increasing attention in recent years due to its inherent advantage of containing more accurate 3D shape information over its 2D counterpart of images. For example, 3D face recognition is expected to be less sensitive to illumination and pose variations because 3D shape of a facial surface is closely related to the unique anatomy of the subject's face and invariant to changes of external environment. Spreeuwers [1] proposed a robust 3D face registration approach, in which 3D point clouds were finely registered by determining a region of interest, and then using the PCA-LDA likelihood classifier and fusion strategy for robust face comparison. Li et al. [2] used 3D keypoint descriptors for 3D face recognition that is robust to pose changes and occlusions. Emambakhsh and Evans [3] developed an expression-robust face recognition approach, in which a set of spherical patches and curves localised over the nasal region of a 3D face were used to select the most stable patches and curves under different facial expressions. These 3D methods achieved higher level of performance and robustness than their 2D counterparts.

Meshes and point clouds, which are interconvertible, are widely used for 3D object representation and registration [4–8]. However, conventional 3D surface matching methods, which match the whole 3D surface meshes or points on 3D scans (see Fig. 1(a)) are both computationally expensive and in high demand of storage space. Moreover, a large number of points on the mesh may not contain discriminative information useful for differentiating an object from others. Therefore, it is crucial to develop efficient and meaningful feature description and matching techniques for 3D object recognition to meet the speed requirement in many real-world applications.

Ridge and valley curves on a 3D surface along which the surface bends sharply are geometrically and perceptually salient surface features that identify areas containing more useful identity information for recognition purpose than flat regions [9,10] (see Fig. 1(b)). Mahoor and Abdel-Mottaleb [11] proposed to encode the range data of a 3D face into a 3D ridge image, which describes the locations of ridge lines around facial regions containing rich identity information (e.g., eyes, nose, and mouth). Then the robust Hausdorff distance (HD) [12] and iterative closet points (ICP) [6] matching mechanisms were utilized to match the 3D curve points between the ridge image of the probe scan and that of the gallery scan. Although the method significantly reduces the computational time and data storage space, it uses only the spatial information of points on 3D curves but ignores the intrinsic structural characteristics implicitly embedded among these curve points.

In this paper, we propose a novel 3D Directional Vertices ($3D^2V$) surface description and matching approach that can greatly reduce the data storage space (to as low as 16% of that is required by the 3D curve-

* Corresponding author.
E-mail address: yongsheng.gao@griffith.edu.au (Y. Gao).

http://dx.doi.org/10.1016/j.patcog.2016.12.009
Received 1 June 2016; Received in revised form 11 December 2016; Accepted 12 December 2016
Available online 14 December 2016

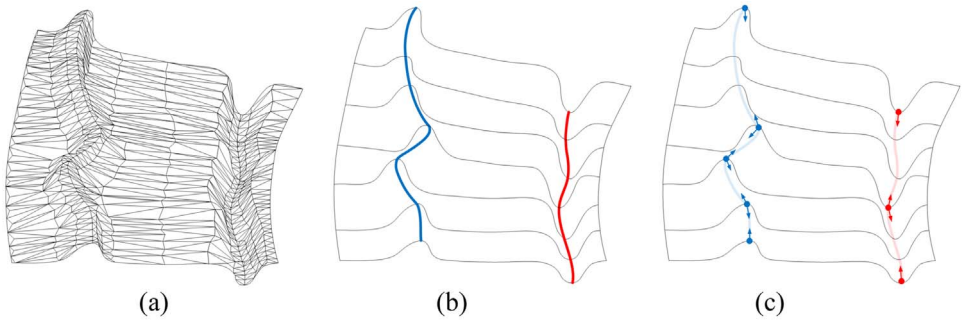

Fig. 1. 3D surface representation by (a) 3D meshes (b) 3D ridge (in blue color) and valley (in red color) curves (c) the proposed 3D directional vertices (points with two or one arrows). (For interpretation of the references to color in this figure legend, the reader is referred to the web version of this article.)

based method [11]) and significantly increase the computation efficiency. Compared to the curve representation as shown in Fig. 1(b), the proposed 3D^{2}Vs (see Fig. 1(c)) are sparsely distributed structured vertices that carry structural information of the curve implicitly embedded in those deleted curve points. Transferring such structural information shared by all points on the curve to only a few points (making them more information bearing structured vertices) and deleting the remaining ones can increase the 3D matching speed and reduce the data storage space, which are important problems to be solved in large scale 3D data matching and retrieval applications. It is very encouraging to observe that the proposed 3D^{2}V representation and matching approach can also increase the recognition accuracy while the data size and computation time are significantly reduced.

The remainder of this paper is organized as follows: Section 2 introduces a new 3D directional vertices (3D^{2}V) representation to characterize 3D surfaces. The proposed 3D^{2}V-to-3D^{2}V correspondence method is discussed in detail. Section 3 presents two set-to-set matching algorithms built from the cost function of 3D^{2}V-to-3D^{2}V conversion. Experimental results on two public databases together with experimental analysis on computational complexity, data size, and sensitivity to parameter are reported in Section 4. Finally, the paper concludes in Section 5.

2. Proposed 3D directional vertices representation and matching

In this paper, we propose a novel 3D surface description and similarity measuring technique, which can effectively harness structural and spatial information around sparse vertices for efficient and accurate recognition of 3D objects. Unlike existing ridge curve [11] and mesh [5,6,8] matching methods, the proposed approach only extracts and matches much less number of structured points on a 3D surface, in which structural relationship information showing connectivity to their neighbours is utilized in establishing the vertex correspondence. Compared to the curve matching techniques, the storage and computation costs are further reduced by using sparse directional vertices instead of all the points on curves.

2.1. Describing 3D surfaces using sparse structured vertices

3D surfaces are represented by continuously connected meshes or dense point clouds (see Fig. 1(a)). In 3D object recognition, only a subset of these surface data contains most of the discriminative information of the object and is important for recognition purposes. For example, the regions of a surface that bend sharply, such as those around eyes, nose and mouth on a 3D face, are geometrically and perceptually salient for characterising the 3D object. 3D curves [11,13,14] are thus proposed for 3D object recognition. They can effectively reduce the computational time and storage demand (see Fig. 1(b)) which is a critical bottleneck for large scale 3D data matching and retrieval tasks. In this study, we propose a novel 3D Directional Vertices (3D^{2}V) representation and matching approach, which uses a few sparsely distributed vertices with structure attributes to minimise the data required for 3D surface matching and also increase the matching accuracy.

After detecting ridge and valley curves [15] on a 3D surface, a fast corner point detection process [16] is applied to the ridge and valley curves to generate 3D^{2}Vs. Let $A(x, y, z, \boldsymbol{n}_1, \boldsymbol{n}_2)$ denote a 3D directional vertex that depicts both the spatial location of the vertex and the structural connectivity information to its neighbours, where (x, y, z) are the Cartesian coordinates of the vertex, $\boldsymbol{n}_1$ and $\boldsymbol{n}_2$ are the unit vectors that point to its two neighbouring vertices on the curve, respectively (see examples in Fig. 1(c)). If a 3D^{2}V is a start point of a curve, a null is assigned to $\boldsymbol{n}_1$. If a 3D^{2}V is an end point of a curve, a null is assigned to $\boldsymbol{n}_2$. A 3D^{2}V is a two-directional vertex with two unit directional vectors pointing to its two neighbouring 3D^{2}Vs or a one-directional vertex (if it is the start/end point of a curve) with a single unit directional vector pointing to its neighbouring 3D^{2}V. These directional vectors provide isolated vertices with additional structural information about the connectivity to their neighbours, which may enhance the discriminative power of the 3D surface descriptor (see an example in Fig. 4). Moreover, the 3D^{2}V descriptor, using sparsely distributed vertices, further reduces the storage demand of a 3D surface representation. Fig. 2 gives an example set of 3D^{2}Vs generated from a 3D face in the FRGC v2.0 database. It can be seen that the 3D surface originally constructed by 14355 mesh points can be characterised by curves formed by 24.4% of the original mesh points (3498 points). The 3D^{2}V descriptor further reduces its point size to only 5.0% of the original mesh points (718 points) through attaching directional attributes to each of them. These attributes carry the structural information implicitly contained in those deleted curve points, and assign such information to the few remaining points in the 3D^{2}V descriptor. This makes the constructed 3D^{2}Vs to be more information bearing structured vertices.

2.2. Establishing 3D^{2}V-to-3D^{2}V correspondence

Let $A(x^A, y^A, z^A, \boldsymbol{n}_1^A, \boldsymbol{n}_2^A)$ and $B(x^B, y^B, z^B, \boldsymbol{n}_1^B, \boldsymbol{n}_2^B)$ be two structured vertices of 3D^{2}Vs, where (x, y, z) is the spatial location of the 3D^{2}V, and unit vectors $\boldsymbol{n}_1$ and $\boldsymbol{n}_2$ are the connectivity vectors of the 3D^{2}V pointing to its two neighbouring vertices, respectively. Their connectivity vectors determine planes $\boldsymbol{\alpha} = k_1\boldsymbol{n}_1^A + k_2\boldsymbol{n}_2^A$ and $\boldsymbol{\beta} = l_1\boldsymbol{n}_1^B + l_2\boldsymbol{n}_2^B$ (k_1, k_2 and l_1, l_2 are constant values) for 3D^{2}V A and 3D^{2}V B respectively, where $\boldsymbol{\alpha} \in \mathbb{R}^3$ and $\boldsymbol{\beta} \in \mathbb{R}^3$ (see Fig. 3(a)). For each 3D^{2}V, a unit vector $\boldsymbol{n} = (\boldsymbol{n}_1 + \boldsymbol{n}_2)/|\boldsymbol{n}_1 + \boldsymbol{n}_2|$ is defined as its principal direction vector for rotation purpose. Thus the principal direction vectors of 3D^{2}V A and 3D^{2}V B, which are plotted in red and blue dashed lines in Fig. 3(a), can be calculated by $\boldsymbol{n}^A = (\boldsymbol{n}_1^A + \boldsymbol{n}_2^A)/|\boldsymbol{n}_1^A + \boldsymbol{n}_2^A|$ and $\boldsymbol{n}^B = (\boldsymbol{n}_1^B + \boldsymbol{n}_2^B)/|\boldsymbol{n}_1^B + \boldsymbol{n}_2^B|$. Note that the principal direction vector of a 3D^{2}V falls in the plane determined by the two connectivity vectors, i.e., $\boldsymbol{n}^A \in \boldsymbol{\alpha}$ and $\boldsymbol{n}^B \in \boldsymbol{\beta}$.

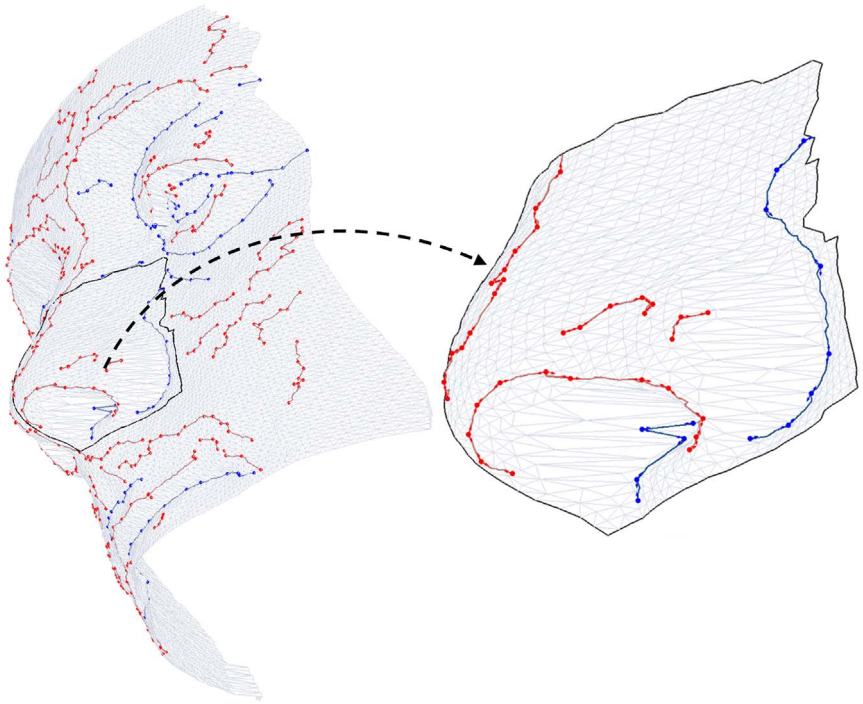

Fig. 2. Visual illustration of an example 3D face using $3D^2Vs$ as primitives. 3D face ID in FRGC v2.0 database: 04225d295; points on mesh triangles: 14355; points on curves: 3498; points in the $3D^2V$ descriptor: 718.

Here, we design a similarity measurement between two individual $3D^2Vs$ that can be used to establish correspondence of $3D^2V$-to-$3D^2V$ from two different objects and effectively measure their difference. Considering both the spatial and structural features of $3D^2Vs$, a multi-operation conversion process is developed to make these two $3D^2Vs$ fully overlapped and the cost of this conversion process is regarded as the dissimilarity between them. More specifically, the difference between these two $3D^2Vs$ is defined as the cost of converting A to B (or vice versa) through a four-operation process consisting of a translation operation, a spin operation, a swing operation and a structure deformation operation. The translation operation moves the spatial location of A to be aligned to that of B. Because every $3D^2V$ is a structured vertex that determines a 2D plane, the spin and swing operations rotate the plan of A to be overlapped with that of B, without changing the structure of either A or B. The structure deformation operation deforms the intrinsic structure of A to be the same as that of B.

1) Translation operation: a translation operation from A to B, denoted as $T(A \rightarrow B)$, moves the spatial location of A to be aligned to the location of B so that $x^A = x^B$, $y^A = y^B$ and $z^A = z^B$ (see changes from Figs. 3(a) to (b)). After that a 2D plane $\boldsymbol{\gamma}$ is created, which is determined by the two principal direction vectors $\boldsymbol{n}^A$ and $\boldsymbol{n}^B$ as illustrated in Figs. 3(b) and (c). The fast L_1 Minkowski distance of this movement is defined as the cost function for a translation operation from A to B:

$$C[T(A \rightarrow B)] = |x^A - x^B| + |y^A - y^B| + |z^A - z^B| \tag{1}$$

2) Spin operation: a spin operation from A to B, denoted as $Sp(A \rightarrow B)$, spins the plane $\boldsymbol{\alpha}$ of structured vertex A around its principal direction vector $\boldsymbol{n}^A$ till the line connecting the end points of $\boldsymbol{n}_1^A$ and $\boldsymbol{n}_2^A$ (i.e. vector $\boldsymbol{n}_1^A - \boldsymbol{n}_2^A$) is parallel to the plane $\boldsymbol{\beta}$ of structured vertex B (see changes from Figs. 3(b) to (c)). The degree of this spin angle is defined as the cost function for a spin operation from A to B:

$$\begin{aligned} C[Sp(A \rightarrow B)] &= cos^{-1}(|(\boldsymbol{n}_1^A - \boldsymbol{n}_2^A)\bullet(\boldsymbol{n}^A \times \boldsymbol{n}^{\boldsymbol{\beta}})|) \\ &= cos^{-1}(|(\boldsymbol{n}_1^A - \boldsymbol{n}_2^A)\bullet(\boldsymbol{n}^A \times (\boldsymbol{n}_1^B \times \boldsymbol{n}_2^B))|) \end{aligned} \tag{2}$$

where $\boldsymbol{n}^{\boldsymbol{\beta}} = \boldsymbol{n}_1^B \times \boldsymbol{n}_2^B$ is the normal vector of plane $\boldsymbol{\beta}$. The absolute value of $(\boldsymbol{n}_1^A - \boldsymbol{n}_2^A)\bullet(\boldsymbol{n}^A \times \boldsymbol{n}^{\boldsymbol{\beta}})$ is used to obtain the smaller intersecting angle as the cost of spin, ensuring the designated cost to remain the same regardless whether or not the order of the two connectivity vectors $\boldsymbol{n}_1^A$ and $\boldsymbol{n}_2^A$ are interchanged.

3) Swing operation: a swing operation from A to B, denoted as $Sw(A \rightarrow B)$, swings the spined plane $\boldsymbol{\alpha}$ of structured vertex A with respect to the origin till it is overlapped with the plane $\boldsymbol{\beta}$ of structured vertex B (see changes from Figs. 3(c) to (d)). During the swing operation, the vector $\boldsymbol{n}^A$ must remain in the plane $\boldsymbol{\gamma}$ and vector $\boldsymbol{n}_1^A - \boldsymbol{n}_2^A$ shall be parallel to the plane $\boldsymbol{\beta}$ when it swings to the position of the vector $\boldsymbol{n}^B$. The degree of this swing angle is defined as the cost function for a swing operation from A to B:

$$C[Sw(A \rightarrow B)] = \cos^{-1}(\boldsymbol{n}^A \bullet \boldsymbol{n}^B) \tag{3}$$

4) Structure deformation operation: an structure deformation operation from A to B, denoted as $D(A \rightarrow B)$, deforms the two directional vectors of A until they coincide with the corresponding directional vectors of B (see changes from Figs. 3(d) to (e)). The amount of this deformation is defined as the cost function for a structure deformation operation from A to B:

$$C[D(A \rightarrow B)] = |\cos^{-1}(\boldsymbol{n}_1^B \bullet \boldsymbol{n}_2^B) - \cos^{-1}(\boldsymbol{n}_1^A \bullet \boldsymbol{n}_2^A)| \tag{4}$$

Together, the overall cost for converting A to B is an aggregated cost of above four operations:

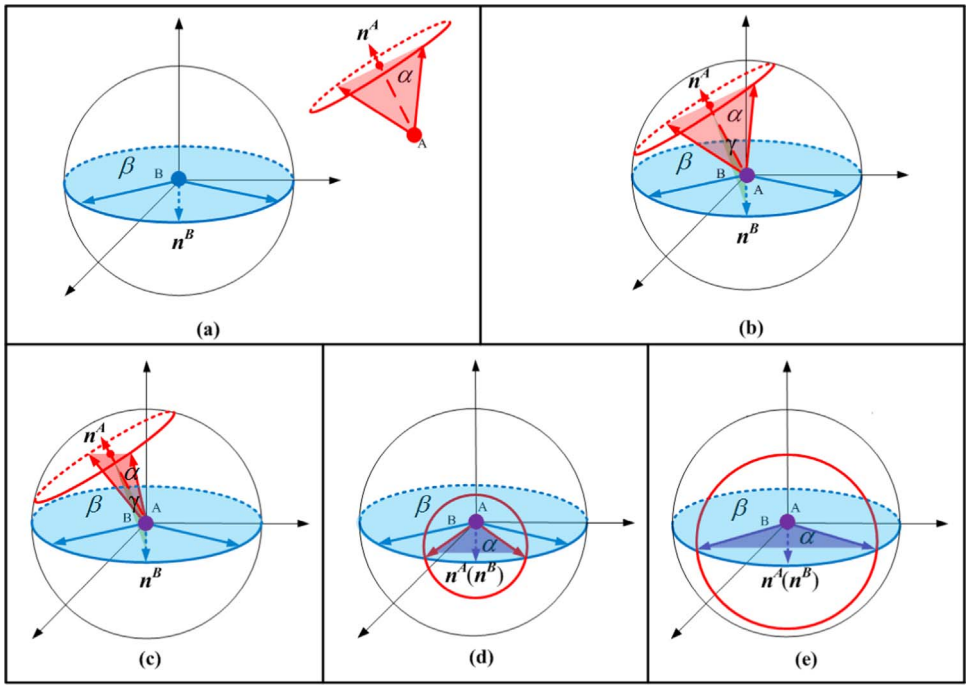

Fig. 3. An illustration of 3D^{2}V-to-3D^{2}V matching process: (a) original states of 3D^{2}Vs A and B, (b) after translation operation, (c) after spin operation, (d) after swing operation, (e) after structure deformation operation. 3D^{2}Vs A and B are in red and blue respectively. Principal direction vectors ($\boldsymbol{n}^A$ and $\boldsymbol{n}^B$) and unit vectors of 3D^{2}Vs are shown by dashed line arrows and solid line arrows respectively. 2D planes $\boldsymbol{\alpha}$, $\boldsymbol{\beta}$, $\boldsymbol{\gamma}$ are marked in light red, blue and green, respectively. Violet color illustrates a region where light red and blue regions become overlapped. (For interpretation of the references to color in this figure legend, the reader is referred to the web version of this article.)

$$C(A \to B) = C[T(A \to B)] + f((C[Sp(A \to B)] + C[Sw(A \to B)]), C[D(A \to B)]) \quad (5)$$

where $f(x, y)$ is a non-linear mapping function for combining two types of heterogeneous costs represented in degree and pixel respectively. Because a small angle of difference tends to be the perturbation (i.e. the intra-class variation) from the same object and a large angle of difference tends to be the inter-class difference, in this paper, an elliptic paraboloid function is used to ignore small angle variations but penalize large angle differences:

$$f(x, y) = \left(\frac{x^2}{a^2} + \frac{y^2}{b^2}\right)/w \quad (6)$$

where w is the weight to balance the contributions of spatial distance measurement and angle difference measurement. Because $C[Sp(A \to B)] \in [0,90°]$, $C[Sw(A \to B)] \in [0,180°]$, $C[D(A \to B)] \in [0,180°)$, we have $x \in [0,270°]$ and $y \in [0,180°)$ respectively. Thus $a = 1.5$ and $b = 1$ are used in $f(x, y)$ to normalize x and y into the same range of $(0,180°)$.

For matching two single-vector 3D^{2}Vs $A(x^A, y^A, z^A, \boldsymbol{n}_i^A)$ and $B(x^B, y^B, z^B, \boldsymbol{n}_j^B)$ where i and j can be either 1 or 2, their spin and structure deformation operations do not exist and the swing operation becomes an action of swing the vector $\boldsymbol{n}_i^A$ of A to be aligned with the vector $\boldsymbol{n}_j^B$ of B along the 2D plane determined by the two vectors of $\boldsymbol{n}_i^A$ and $\boldsymbol{n}_j^B$. The cost function for a swing operation between two single-vector 3D^{2}V is defined as

$$C[Sw(A \to B)] = \cos^{-1}(\boldsymbol{n}_i^A \bullet \boldsymbol{n}_j^B) \quad (7)$$

Thus, the cost function of matching two single-vector 3D^{2}Vs becomes

$$C(A \to B) = C[T(A \to B)] + f(C[Sw(A \to B)], 0) \quad (8)$$

where $C[T(A \to B)]$ is the same as defined in Eq. (1).

It is desirable to penalize matching between two 3D^{2}Vs of different types. We set $C[Sp(A \to B)]$, $C[Sw(A \to B)]$, and $C[D(A \to B)]$ to their maximum values of 90°, 180° and 180° respectively when matching a single-vector 3D^{2}V to a two-vector 3D^{2}V or vice versa. Thus the total cost function of matching two 3D^{2}Vs of different types becomes

$$C(A \to B) = C[T(A \to B)] + f(90° + 180°, 180°) \quad (9)$$

Fig. 4 gives an example illustrating the effectiveness and difference of point correspondence in the proposed 3D^{2}V matching in comparison with that in the existing 3D curve-based matching [11]. Given a point a on a 3D curve of gallery $\boldsymbol{G}$, and three points b_1, b_2, and b_3 on 3D curves of probe $\boldsymbol{P}$ (see Fig. 4(a)), it is clear that a in $\boldsymbol{G}$ shall be matched to b_1 in $\boldsymbol{P}$ due to the high similarity of their curves. The 3D curve-based matching will mis-identify b_2 as the corresponding point of a (see Fig. 4(a) and (b)) because b_2 is slightly closer to a than the other two points although they are structurally very different. However, if encoding the 3D curves into sparse 3D^{2}Vs (see Fig. 4(c)), the point correspondence is established by finding the pair with minimum conversion cost calculated using Eq. (5). Let $C[S(A \to B)]$ denote the cost of structural conversion operation $f((C[Sp(A \to B)] + C[Sw(A \to B)]), C[D(A \to B)])$. Although $C[T(A \to B_2)] < C[T(A \to B_1)] = R < C[T(A \to B_3)]$, we have $C[S(A \to B_1)] = 0 < C[S(A \to B_2)]$ and $C[S(A \to B_1)] = 0 < C[S(A \to B_3)]$ (see Fig. 4(d)), which results in $C(A \to B_1) < C(A \to B_2)$, $C(A \to B_1) < C(A \to B_3)$ and correctly identifies B_1 as the corresponding 3D^{2}V of A.

3. Set-to-set dissimilarity measurement

In this study, we developed two global matching algorithms for measuring the dissimilarity between two 3D^{2}V sets using Hausdorff distance (HD) and iterative closest point (ICP) mechanisms respectively. In order to compare directly with the 3D ridge curve method, both of them are implemented in the similar way as in the benchmark method [11] without employing any other performance improvement tricks/techniques.

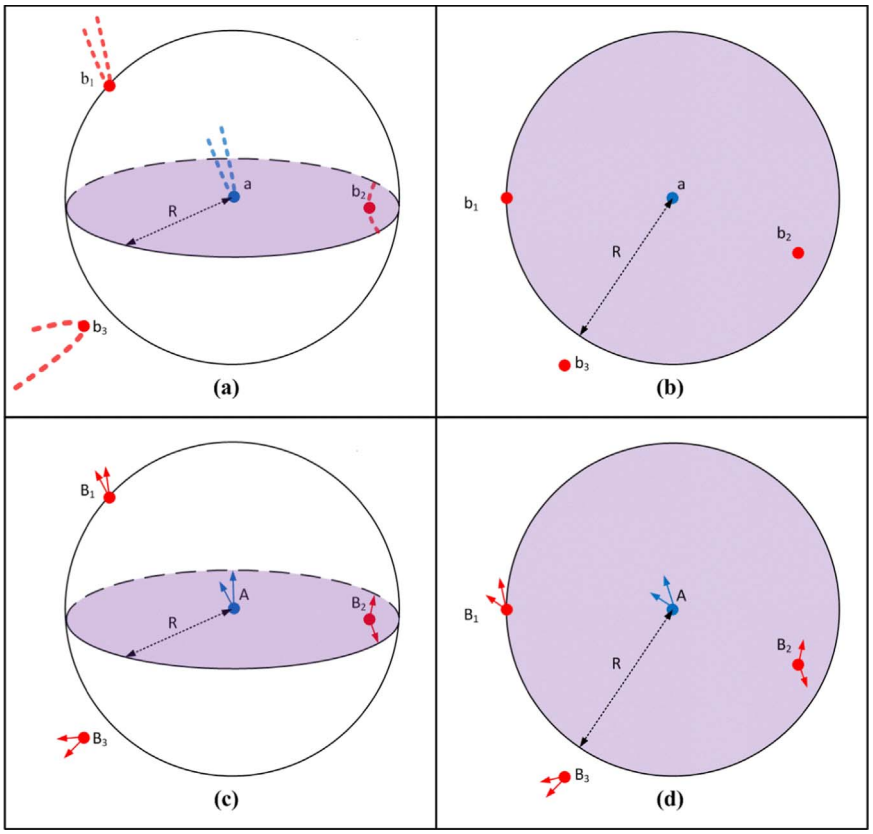

Fig. 4. An example illustrating the correspondence process of the proposed 3D^{2}V method in comparison with that of the 3D curve-based method [11]: (a) 3D curve points in 3D space, (b) 3D curve points projected onto a 2D plane, (c) 3D^{2}Vs in 3D space, (d) 3D^{2}V points projected onto a 2D plane. 3D curve point a and it corresponding 3D^{2}V A in the gallery $\boldsymbol{G}$ are marked in blue color, and 3D curve points b_1, b_2, b_3 and their corresponding 3D^{2}Vs B_1, B_2, B_3 in the probe $\boldsymbol{P}$ are marked in red color. (For interpretation of the references to color in this figure legend, the reader is referred to the web version of this article.)

3.1. Matching two 3D^{2}V sets by HD mechanism

Given two finite 3D^{2}V sets $\boldsymbol{G} = \bigcup_k \boldsymbol{G}^k = \left\{A_1^1, A_2^1, \ldots, A_{N_G^1}^1, \ldots, A_1^K, A_2^K, \ldots, A_{N_G^K}^K\right\}$ and $\boldsymbol{P} = \bigcup_k \boldsymbol{P}^k = \left\{B_1^1, B_2^1, \ldots, B_{N_P^1}^1, \ldots, B_1^K, B_2^K, \ldots, B_{N_P^K}^K\right\}$ representing gallery and probe 3D objects respectively. Each 3D^{2}V set is comprised of K 3D^{2}V subsets. K is the number of types of 3D^{2}Vs (In our experiments, K is set as 2 where $k = 1$ denotes a ridge type 3D^{2}V and $k = 2$ denotes a valley type 3D^{2}V). N_G^k and N_P^k are the numbers of 3D^{2}Vs in the kth subsets $\boldsymbol{G}^k$ and $\boldsymbol{P}^k$ respectively. For each 3D^{2}V A_i^k in subset $\boldsymbol{G}^k$, its corresponding 3D^{2}V B_j^k in subset $\boldsymbol{P}^k$ is identified as the one with minimum conversion cost from A_i^k to B_j^k among all $B_j^k \in \boldsymbol{P}^k$. Note that A_i^k in subset $\boldsymbol{G}^k$ can only find its correspondence in the 3D^{2}Vs of the same type, that is in the subset of $\boldsymbol{P}^k$ with the same type index k. The cost for establishing the correspondence for A_i^k can be calculated by

$$C(A_i^k) = \min_{B_j^k \in \boldsymbol{P}^k} C(A_i^k \rightarrow B_j^k) \tag{10}$$

The least trimmed square strategy [17] is used in our design to alleviate the problem of outliers in 3D data and from segmentation process. The cost for converting subset $\boldsymbol{G}^k$ in $\boldsymbol{G}$ to subset $\boldsymbol{P}^k$ in $\boldsymbol{P}$, denoted as $\boldsymbol{G}^k \Rightarrow \boldsymbol{P}^k$, is defined as

$$C(\boldsymbol{G}^k \Rightarrow \boldsymbol{P}^k) = \frac{1}{H}\sum_{i=1}^{H} C(A_i^k) = \frac{1}{H}\sum_{i=1}^{H} \min_{B_j^k \in \boldsymbol{P}^k} C(A_i^k \rightarrow B_j^k) \tag{11}$$

where $H = h \times N_G^k$ $(0 \le h \le 1)$, N_G^k is the number of 3D^{2}V A_i^k in subset $\boldsymbol{G}^k$, h is the percentage of 3D^{2}Vs to be kept for calculating the cost, and $C(A_i^k)$ for $i = 1, 2, \ldots, N_G^k$ are sorted in ascending order as a sequence of $C(A_1^k) \le C(A_2^k) \le \cdots \le C(A_{N_G^k}^k)$. The measure is calculated by eliminating the large conversion cost values which tend to be generated from outliers and only keeping the h percent of the smallest conversion costs. In our experiments, the value of h is set heuristically to 80%.

Finally, the dissimilarity between subset $\boldsymbol{G}^k$ and subset $\boldsymbol{P}^k$ is defined as the maximum of the two minimum costs that establish correspondences from subset $\boldsymbol{G}^k$ to subset $\boldsymbol{P}^k$ and subset $\boldsymbol{P}^k$ to subset $\boldsymbol{G}^k$ respectively. The dissimilarity between gallery and probe scans, noted as $D(\boldsymbol{G}, \boldsymbol{P})$, is defined as the aggregated cost using score-level fusion by summing all the subset-to-subset dissimilarity scores $D(\boldsymbol{G}^k, \boldsymbol{P}^k)$ for all types of 3D^{2}Vs:

$$D(\boldsymbol{G}, \boldsymbol{P}) = \sum_{k=1}^{K} D(\boldsymbol{G}^k, \boldsymbol{P}^k) = \sum_{k=1}^{K} \max[C(\boldsymbol{G}^k \Rightarrow \boldsymbol{P}^k), C(\boldsymbol{P}^k \Rightarrow \boldsymbol{G}^k)] \tag{12}$$

3.2. Matching two 3D^{2}V sets by ICP mechanism

The iterative closest point (ICP) [6] is a widely adopted method to deal with the rigid registration problem. It involves two processes: 1) establishing correspondence between two point sets; 2) computing the transformation under which one point set aligns with the other one. Different variants of ICP have been proposed, which use unique techniques for selecting and matching points, and minimizing the error of estimation [18].

In this study, the ICP matching mechanism with outlier rejection [19] is also used in implementing the matching algorithm of the proposed 3D^{2}V approach (see Algorithm 1) and comparing its perfor-

mance against the 3D curve-based benchmark method [11]. During each iteration of ICP registration, the 3D^{2}V pairs are established by finding the closest point from one object to the other. A distance threshold is implemented to reject outlier pairs. Rigid transforms are then determined by a point-to-point error metric. After terminating the iteration process and obtaining the optimal rigid transforms, the average conversion cost between the selected 3D^{2}V corresponding pairs are used to measure the dissimilarity between gallery and probe scans.

Algorithm 1. Set-to-set 3D^{2}V matching algorithm using ICP mechanism.

Input: two 3D^{2}V sets $\boldsymbol{G} = \bigcup_k \boldsymbol{G}^k = \left\{A_1^1, A_2^1, \ldots, A_{N_G^1}^1, \ldots, A_1^K, A_2^K, \ldots, A_{N_G^K}^K\right\}$ and $\boldsymbol{P} = \bigcup_k \boldsymbol{P}^k = \left\{B_1^1, B_2^1, \ldots, B_{N_P^1}^1, \ldots, B_1^K, B_2^K, \ldots, B_{N_P^K}^K\right\}$, where N_G^k and N_P^k are the numbers of 3D^{2}Vs in subsets $\boldsymbol{G}^k$ and $\boldsymbol{P}^k$ respectively. K is the number of types of 3D^{2}Vs.

Initialization: distance threshold τ (=4 in our experiments), maximum number of iteration $iter_{max}$ (=10 in our experiments), translation vector $\boldsymbol{T} = \begin{bmatrix}0\\0\\0\end{bmatrix}$, and rotation matrix $\boldsymbol{R} = \begin{bmatrix}1&0&0\\0&1&0\\0&0&1\end{bmatrix}$.

1: for $t = 1, \ldots, iter_{max}$

2: establish the correspondence of point sets using the $(t-1)^{\text{th}}$ transformations $\boldsymbol{T}$ and $\boldsymbol{R}$.

$$\hat{A}_i^k = arg \min_{j\in 1,2,\ldots,N_G^k} \|B_i^k - [\boldsymbol{R}(A_j^k) + \boldsymbol{T}]\|$$

For each 3D^{2}V B_i^k in subset $\boldsymbol{P}^k$, find the closest 3D^{2}V $\hat{A}_i^k$ from the subset $\boldsymbol{G}^k$ using the Euclidian distance to build an estimated correspondence pair. If the distance between $\hat{A}_i^k$ and B_i^k is larger than τ, it will be considered as an outlier and discarded.

3: compute the t^{th} transformations $\boldsymbol{T}$ and $\boldsymbol{R}$ that minimise the mean square error (MSE) of the estimated correspondence pairs:

$$MSE = \frac{1}{\hat{N}_P} \sum_{k=1}^{K} \sum_{i=1}^{\hat{N}_P^k} \|B_i^k - [\boldsymbol{R}(\hat{A}_i^k) + \boldsymbol{T}]\|^2$$

where $\hat{N}_P = \sum_{k=1}^{K} \hat{N}_P^k$, and $\hat{N}_P^k$ is the number of estimated correspondence pair in subset $\boldsymbol{P}^k$ of the probe scan.

4: if the change of MSE is sufficiently small (smaller than 0.01 in our experiments), terminate the iteration.

Output: the average conversion cost for all $\hat{N}_P$ estimated 3D^{2}V pairs from $\boldsymbol{P}$ to $\boldsymbol{G}$.

$$Cost = \frac{1}{\hat{N}_P} \sum_{k=1}^{K} \sum_{i=1}^{\hat{N}_P^k} C(B_i^k \rightarrow [\boldsymbol{R}(\hat{A}_i^k) + \boldsymbol{T}])$$

4. Experimental results

The effectiveness and efficiency of the proposed 3D^{2}V method are evaluated and compared directly with its counterpart that uses 3D curves [11]. In order to have a fair and direct comparison with the proposed method, the 3D curve-based benchmark method in the following experiments uses both ridge and valley curves, instead of only the ridge curves as in [11]. The comparative experiments are conducted on two publicly available 3D face databases, GavabDB [20] and FRGCv2.0 [21]. All the 3D faces are normalized and cropped by a pre-processing step as described in [22]. No performance enhancement techniques are used in this study to ensure a fair and direct comparative study of the competing techniques.

In our experiments, ridge and valley curves are detected using [15] which consists of three steps: 1) estimate the principal curvature tensor and derivatives, 2) trace the ridge and valley curves, and 3) efficiently threshold the curves. After detecting ridge and valley curves on a 3D surface, the fast corner point detection algorithm [16] is applied to generate 3D^{2}Vs, in which a constant threshold is employed to control the maximum error between the original curves and the generated polygonal lines. However, the proposed method in this paper is not limited to using above particular algorithms for generating 3D^{2}Vs. In theory, any ridge/valley detection and corner detection algorithms can be used.

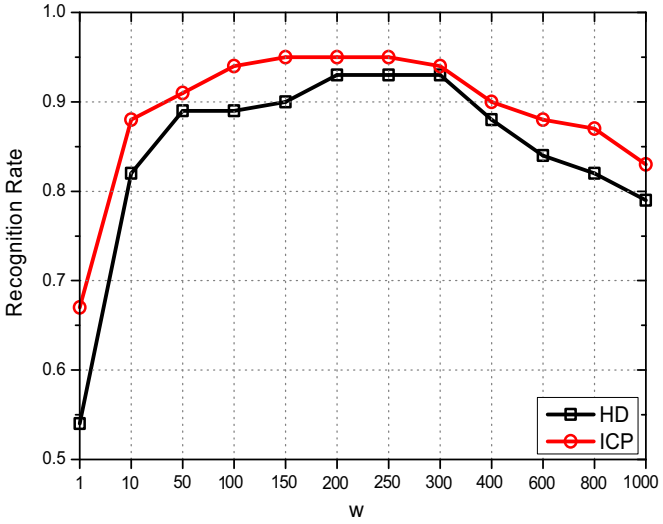

Fig. 5. The effect of w on recognition rate.

4.1. Determination of parameter w

In this section, we investigate the effect and sensitivity of parameter w in Eq. (6) on the recognition accuracy. In theory, the parameter w is a weight used to balance the contributions from the spatial translation distance and the local structural difference between two 3D^{2}Vs to be matched. When the value of w is small, the contribution of the spatial translation distance to the overall cost for converting one 3D^{2}V to the other is small. With the increase of w, the contribution from the translation distance increases.

The first 100 people with at least two neutral 3D faces per person from the FRGC v2.0 Spring2003 dataset were used in our parameter sensitivity analysis. The neutral 3D face in the first replicate subject session was used as the gallery of the person, and the neutral 3D face in the second replicate subject session was used as the probe. The recognition rates (calculated using the nearest neighbour classification with the defined matching cost) of the proposed method using both HD and ICP matching mechanisms are plotted against the values of w in Fig. 5. It is observed that, using HD and ICP matching mechanisms, the proposed 3D^{2}V method achieved 54% and 67% respectively when w=1. Their performances increased quickly and reached the optimal value of 93% and 95% when w became 200 (for HD matching scheme) and 150 (for ICP matching scheme), and remained stable till 300 and 250 respectively. For the rest of the experiments in this paper, we set w as 200.

4.2. Experiments on FRGC 2.0 face database

In this section, we conducted comparative experiments on the FRGC v2.0 database [21], which is one of the largest 2D and 3D face databases. The FRGC database contains 4950 3D face scans acquired with the Minolta Vivid scanner, in the presence of minor pose variations and major illumination and expression variations. The database is divided into three sets based on acquisition time: Spring2003, Fall2003, and Spring2004. The Spring2003 is specified

Fig. 6. Examples of normalized 3D face scans in the FRGC v2.0 database [21]. For each column, the upper one is the gallery scan while the bottom one is the probe scan from the same subject.

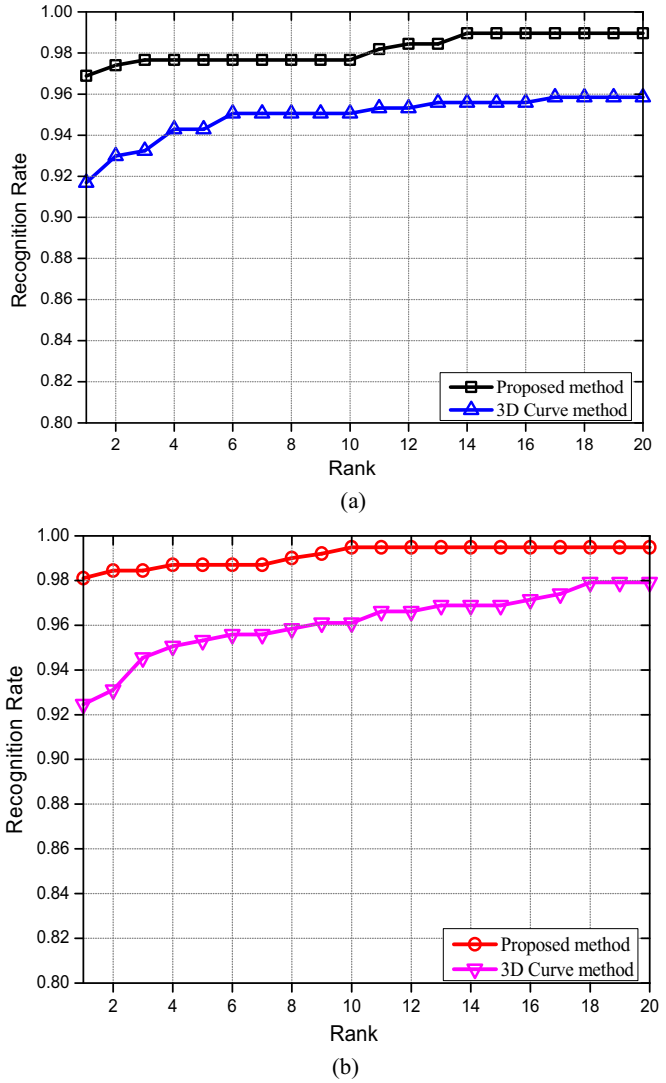

Fig. 7. Comparison of CMC curves between the proposed 3D^{2}V method and the 3D curve method [11] obtained from the "neutral vs. neutral" identification experiments on FRGC v2.0 database. (a) The results obtained using the HD matching mechanism and (b) the results obtained using the ICP matching mechanism.

as the training set, while the Fall2003 and Spring2004 are specified as the validation sets. In our experiments, we used all the 2410 3D face scans with neutral expression (466 gallery faces and 1944 probe faces) from the validation sets (Fall2003 and Spring2004). Both identification and verification experimental protocols were used for evaluating the performance of the algorithms.

For the identification experiments, the 385 subjects which have at least two 3D scans were selected. For each subject, the first scan was used as the gallery while the second scan was used as the probe (see examples in Fig. 6). Each probe was matched against all the galleries of the 385 subjects. Note that this was a single gallery identification experiment, in which each person was represented by only a single 3D scan. The cumulative match characteristic (CMC) curve [23–25], which judges the ranking capabilities of an identification system, was used for performance measurement. For an identification test, the CMC curve plots the recognition rates against ranks that are used to determine how a correct match is counted. In rank N matching, a correct match is counted only when the gallery face from the same person as the probe face is among the best N matched gallery faces. Fig. 7 shows the CMC curves of the proposed method and the benchmark method. Although the proposed method only uses a significantly smaller sized feature data that is only 16.0% of curve points used by the benchmark method [11] (see Section 4.4), its CMC curve is much higher than that of the 3D curve based benchmark with a noticeable margin for both HD and ICP matching mechanisms. Note that the proposed method achieved 96.9% (for HD matching scheme) and 98.2% (for ICP matching scheme) rank-1 identification accuracy, which outperformed the benchmark method by 5.2% and 5.7% respectively.

Our verification experiments adopted the standard FRGC ROC III

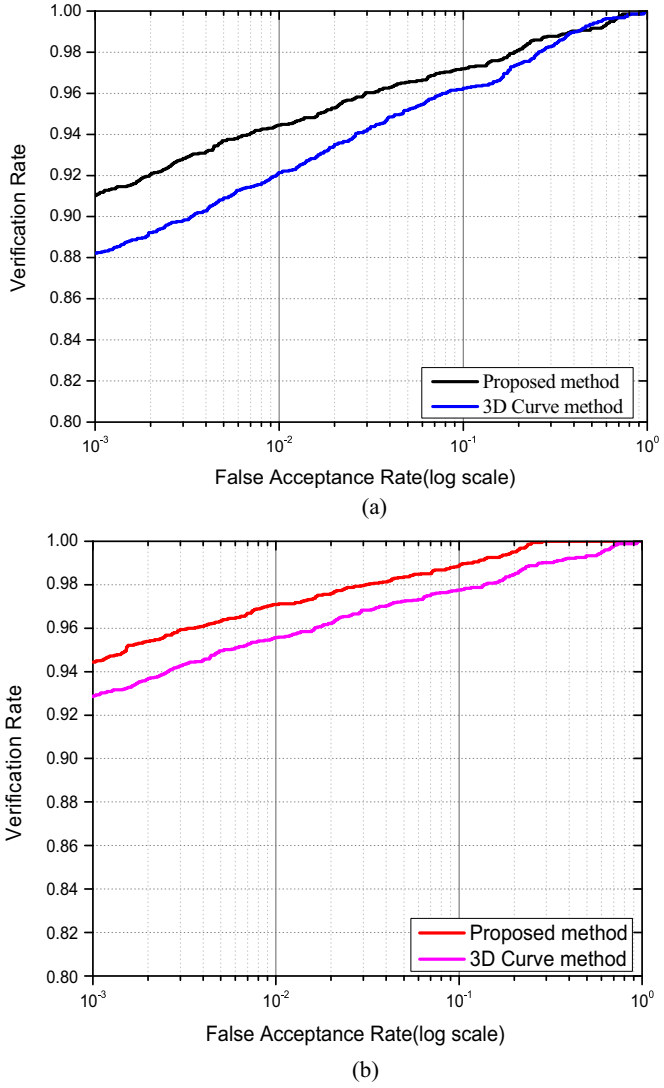

Fig. 8. Comparison of ROC curves between the proposed 3D^{2}V method and the 3D curve method [11] obtained from the "neutral vs. neutral" verification experiments that follow the FRGC ROC III protocol [21]. (a) The results obtained using the HD matching mechanism and (b) the results obtained using the ICP matching mechanism.

protocol [21], in which the 1060 3D scans collected in the Fall2003 were used as galleries and the 1350 3D scans collected in the Spring2004 were used as probes. The time difference between taking the galleries in Fall2003 and taking the probes in Spring2004 of the same subject varies from two to ten months. The Receiver Operating Characteristic (ROC) curves [24,26,27] illustrating the trade-off between verification and false acceptance rates are plotted in Fig. 8. For a verification test, the ROC curve is a plot of the verification rates (also called true positive rates) against the false positive rates that are computed at different thresholds. Consistent to the results obtained from the identification experiments, the proposed method achieved a higher ROC curve than that of the 3D curve method with an obvious margin for both HD and ICP matching schemes. The proposed method obtained 91.1% (for HD matching scheme) and 94.5% (for ICP matching scheme) of verification rate at 0.1% false acceptance rate (FAR), outperforming the benchmark method by 2.9% and 1.7% respectively.

4.3. Experiments on GavabDB database

Comparative experimental study is also conducted on the GavabDB database [20] with 3D face scans acquired using a Minolta Vi-700 laser scanner. The database contains a total of 549 3D face scans from 61 subjects (45 males and 16 females). Each subject was scanned nine times from different angles and under different facial expressions (two neutral expression frontal scans, two neutral expression scans with looking down and up poses, three frontal scans with smile, laugh, and an arbitrary expression chosen freely by the subject, and two profile scans).

The first frontal 3D scan with neutral expression was taken as the gallery of the subject, and the remaining six 3D scans were used as probes (except the 2 profile scans). There were 427 3D scans in total (61 used as galleries and 366 used as probes) in our experiment. Fig. 9 shows two sets of normalized 3D face scans from two subjects in the GavabDB database. The leftmost scan in each row is the gallery scan of the subject. Unlike the benchmark method [11] that used an iterative HD matching mechanism to handle the imperfect alignment problem and concerned only the upper part of 3D face scans when matching 3D scans with facial expressions to eliminate negative impact of large expression variation around mouth region, we ignored all these accuracy improvement tricks for pure comparison of algorithms.

Fig. 10 gives the Cumulative Matching Characteristic (CMC) curves of the proposed method and the 3D curve-based benchmark method using both HD and ICP matching mechanisms. Similar to the "neutral vs. neutral" experimental results obtained on the FRGC v2.0 database, the proposed method performed better than the curve-based benchmark method in the "all vs. neutral" identification experiment. Our approach achieved average rank-1 identification accuracies of 80.1% and 87.9% with HD and ICP matching mechanisms respectively, outperforming the benchmark method by 6.0% and 5.5% respectively.

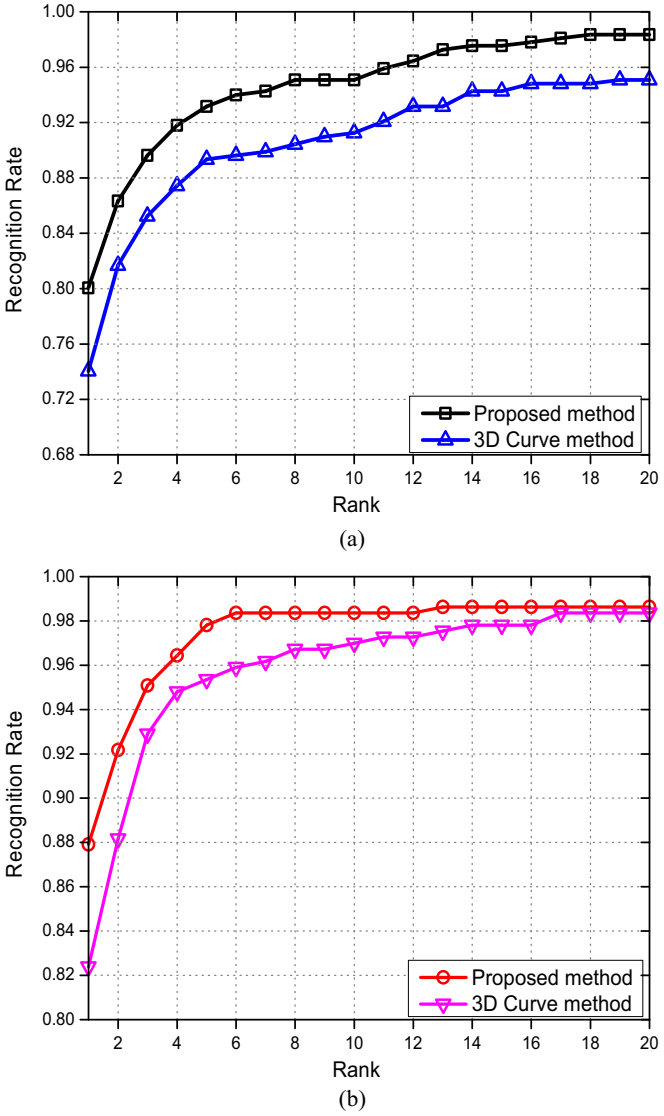

Fig. 10. Comparison of CMC curves between the proposed 3D^{2}V method and the 3D curve method [11] obtained from the "all vs. neutral" identification experiments on GavabDB database. (a) The results obtained using the HD matching mechanism and (b) the results obtained using the ICP matching mechanism.

To further analyse the performance of the proposed approach, we separated the probes into a neutral set (the second frontal neutral expression scan, the neutral scan with looking down pose, and the

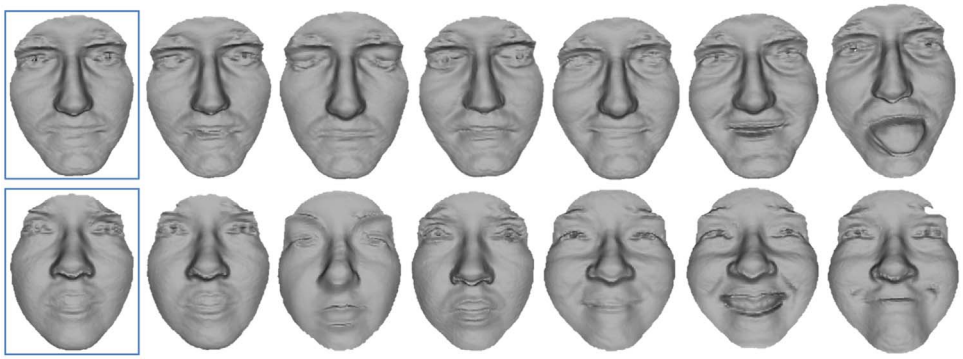

Fig. 9. Examples of normalized GavabDB 3D face scans used in our comparative experiments. For each subject (displayed in a row), the leftmost (frontal scan with neutral expression) was used as the gallery and the remaining 6 (the other neutral expression frontal scan, a neutral expression scan with looking down pose, a neutral expression scan with looking up pose, and three frontal scans with smile, laugh, and an arbitrary expression chosen freely by the subject) were used as the probes.

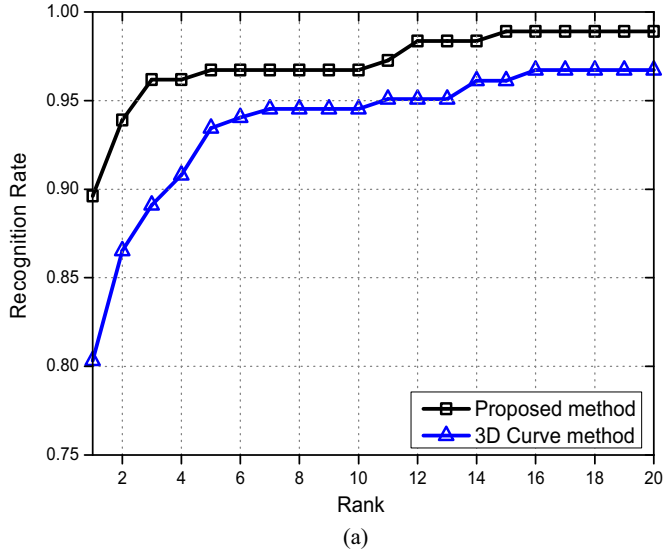

Fig. 11. Comparison of CMC curves between the proposed 3D^{2}V method and the 3D curve method [11] obtained from the "neutral vs. neutral" identification experiments on GavabDB database. (a) The results obtained using the HD matching mechanism and (b) the results obtained using the ICP matching mechanism.

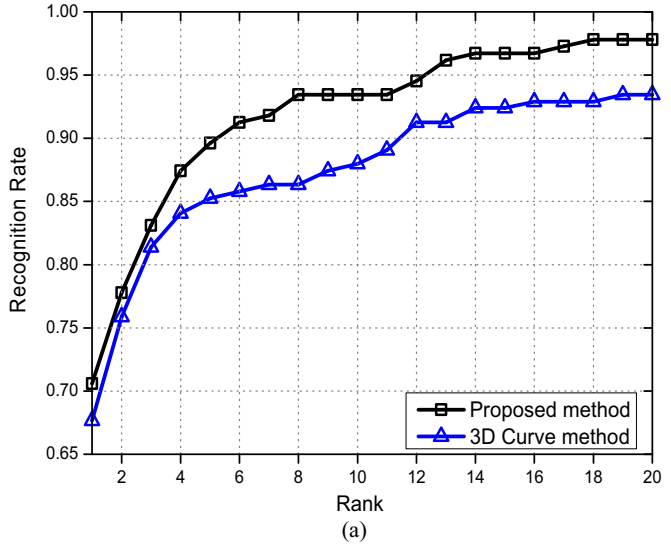

Fig. 12. Comparison of CMC curves between the proposed 3D^{2}V method and the 3D curve method [11] obtained from the "expressive vs. neutral" identification experiments on GavabDB database. (a) The results obtained using the HD matching mechanism and (b) the results obtained using the ICP matching mechanism.

neutral expression scan with looking up pose) and an expressive set (the three frontal scans with different expressions). Using the first frontal neutral expression scan as the only gallery for each person, we conducted a single model "neutral vs. neutral" identification test and a single model "expressive vs. neutral" identification test. The Cumulative Matching Characteristic (CMC) curves of the proposed method and the 3D curve-based benchmark method using both HD and ICP matching mechanisms are shown in Figs. 11 and 12, respectively.

In the "neutral vs. neutral" identification test, our approach achieved average rank-1 identification accuracies of 89.6% and 95.6% with HD and ICP matching mechanisms respectively, outperforming the benchmark method by 9.3% and 8.2% respectively. Similarly, in the "expressive vs. neutral" identification test, our approach obtained average rank-1 identification accuracies of 70.5% and 79.8% with HD and ICP matching mechanisms respectively, outperforming the benchmark method by smaller margins of 2.7% and 2.8% respectively.

These results demonstrate that using only a few sparsely distributed vertices with structure attributes can effectively minimise the data required for 3D surface matching and also increase the matching accuracy.

Table 1
Comparison of average data size on the FRGC v2.0 database.

	3D curve [11]	3D^{2}V
Average number of (feature) points	3888	623
Percentage of original 3D data size	29.8%	4.8%

4.4. Storage and computational complexity

The storage requirement of the proposed 3D^{2}V method is analysed and compared with the 3D curve method [11] using all the 2410 scans with neutral expression in the validation set of FRGC v2.0 database. The results are summarised in Table 1. On average, the 3D curve method uses 3888 point, 29.8% of the original mesh points to represent a 3D face scan. The proposed 3D^{2}V descriptor further reduces its data size to 623 points, only 16.0% of the storage space that is required by the 3D curve benchmark and 4.8% of the original mesh points. It is worth stressing that compared to the 3D curve benchmark method [11], the 84.0% reduction of storage space is achieved together with an accuracy increase of 5.2% (for HD matching mechanism) and 5.7% (for

Table 2
Comparison of average computational time on the FRGC v2.0 database.

Approach	HD	ICP
3D curve matching [11]	0.83 s	2.66 s
3D^{2}V matching	0.35 s	0.46 s
Reduction in time (%)	57.8%	82.7%

ICP matching mechanism) (see Section 4.2). This improvement ought to be attributed to, as discussed in Section 3, the fact that the 3D^{2}Vs carry the structural information implicitly contained in those deleted curve points, which makes them more information bearing structured vertices for effective 3D surface matching.

The computational complexities of the proposed 3D^{2}V method and the 3D curve method [11] are of the order $O(p_v q_v t_v)$ and $O(p_c q_c t_c)$ respectively. p_v and q_v are the numbers of 3D^{2}Vs in probe and gallery scans, while p_c and q_c are the numbers of 3D curve points in probe and gallery scans. t_v and t_c are the time to compute the 3D^{2}V-to-3D^{2}V conversion cost in 3D^{2}V matching and the Euclidean distance in 3D curve matching [11], respectively. Table 2 gives the actual average computational time of the proposed 3D^{2}V matching method and 3D curve matching method by using both HD and ICP mechanisms obtained on the FRGC v2.0 database. All the reported time was obtained by algorithms implemented using MATLAB running on a PC with an INTEL Core i5 3.2 GHz and 4 GB RAM. Our approach requires on average only 0.35 s for matching a single probe with a gallery dataset of 466 3D face scans (1-to-466 matching) under HD matching mechanism while the 3D curve benchmark method takes an average of 0.83 s to match against the same dataset. A 57.8% reduction of computation time is achieved. The time difference is greater when using ICP matching mechanism, with 0.46 s and 2.66 s respectively, which translate into an 82.7% reduction of computation time. Since the time (t_v) of calculating the 3D^{2}V-to-3D^{2}V conversion cost is larger than the time (t_c) of calculating a simple Euclidean distance in the 3D curve method, we have

$$\frac{O(p_v q_v t_v)}{O(p_c q_c t_c)} > \frac{O(p_v q_v)}{O(p_c q_c)}.$$

With some acceleration techniques (such as, hardware acceleration or look up table), the time of calculating 3D^{2}V-to-3D^{2}V conversion cost can be reduced by minimizing t_v. When $t_v \approx t_c$, the computation time of 3D^{2}V matching would be approaching to only about 3% of the time needed for 3D curve matching [11]:

$$\frac{p_v}{q_v} \bullet \frac{q_v}{q_c} < (16.0\%)^2 < 3\%$$

This is equivalent to a 97% reduction of time, which is the ideal upper bound of computational time reduction for the proposed 3D^{2}V matching method with respect to the 3D curve matching benchmark method [11].

4.5. Sensitivity to noise and number of 3D^{2}Vs

In this section, we used the GavabDB database to analyse the sensitivity to noise of the proposed method. The first frontal scan with neutral expression in the database was used as the single gallery of each person, while the second frontal scan with neutral expression was used as the probe. All probe scans were randomly perturbed by adding a Gaussian noise with zero mean and varying standard deviation ($\mu = 0$, $\sigma = 1,2,3,4$) to the depth of the point clouds on the 3D facial surfaces (see examples in the bottom row of Fig. 13). Fig. 13 illustrates the rank-1 recognition rates of the proposed method obtained on the 3D surfaces corrupted by various levels of noise. It is found that the

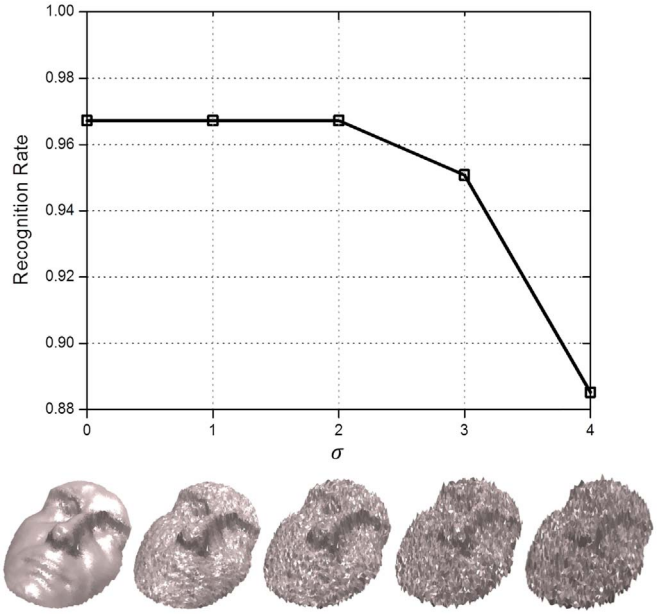

Fig. 13. Rank-1 recognition rates of the proposed method by using HD matching mechanism on 3D faces from the GavabDB database (neutral vs. neutral) corrupted by different levels of Gaussian noise.

recognition rate remained stable at 96.72% till $\sigma = 2$, when the 3D surfaces were already obviously corrupted. When the noise level continued to increase, the recognition rate started decreasing to 95.08% for $\sigma = 3$ and dropped significantly from $\sigma = 4$ when the facial components (e.g., mouth, nose and eyes) become difficult to identify.

A sensitivity evaluation to varying number of 3D^{2}Vs was also conducted in this study. In our implementation, the number of 3D^{2}Vs was controlled by a threshold parameter λ in the corner detection algorithm as described in the beginning of Section 4. When the value of λ is small, more corner points are detected from the original curves and thus more 3D^{2}Vs are generated. The number of 3D^{2}Vs (and thus the storage space and computational time) can be reduced by increasing the value of λ.

Same as the experiment in Section 4.1, the first 100 subjects with at least two neutral 3D faces per person from the FRGC v2.0 Spring2003 dataset were used, where the neutral 3D face scan in the first replicate subject session was used as the gallery of the person, and the neutral 3D face scan in the second replicate subject session was used as the probe. The recognition rates of the proposed method using both HD and ICP mechanisms with varying number of 3D^{2}Vs, which are also described by the percentage of the original 3D mesh points and percentage of the 3D curve points respectively, are summarised in Table 3. When the average number of 3D^{2}Vs changes from 2157 to 422

Table 3
The effect of number of 3D^{2}Vs on recognition rate. The data in bold indicate the parameters used in all other comparative experiments.

λ	0.1	0.2	0.4	**0.6**	0.8	1
Average number of 3D^{2}Vs	2157	1563	927	**623**	511	422
Average percentage of original 3D data size	16.6%	12.0%	7.1%	**4.8%**	3.9%	3.2%
Average percentage of curve points	55.6%	40.3%	23.9%	**16.1%**	13.2%	10.9%
HD matching mechanism	94%	95%	94%	93%	94%	93%
ICP matching mechanism	95%	95%	95%	95%	95%	95%

(that is, 16.6–3.2% of the original 3D mesh points, 55.6–10.9% of the 3D curve points), the recognition rates of the proposed method using both HD and ICP matching mechanisms remained stable with only 1% of variation. Note that the number of $3D^2Vs$ used in all the other experiments of this paper (highlighted in bold) is reasonably chosen.

5. Conclusion

Large storage space requirement and expensive computational cost are two major technical barriers in developing 3D data matching and retrieval application systems. In this paper, we present a new tool that can be used for developing more efficient 3D surfaces matching algorithms. Derived from ridge and valley curves, the proposed 3D directional vertices ($3D^2V$) representation and matching approach can effectively employ both spatial and structural information on 3D surfaces with much less data and running time.

The proposed method has been evaluated on the FRGC v2.0 and GavabDB databases and been compared with the 3D ridge curve benchmark method. The experimental results show that the proposed $3D^2V$ method can significantly reduce the data storage demand to only 16% of the storage space required by the 3D curve benchmark method, which is a merely 4.8% of the mesh points in original 3D scan data. Computational time is reduced to 42% (using HD matching scheme) and 17% (using ICP matching scheme) of that required by the 3D curve benchmark method. It is very encouraging to find that the proposed method also achieved a recognition accuracy increase of 5.2–6.0% at the same time with above significant reductions of data storage space and computational time. This attests that the added directional features of $3D^2Vs$ together with their four conversion operation matching approach can effectively improve discriminating power. This study reveals that $3D^2Vs$ can provide an efficient solution for 3D surface matching, which may find its application in general 3D object representation and recognition.

Acknowledgements

This work is partially supported by Australian Research Council (ARC) under Discovery Grants DP0877929 and DP140101075.

References

[1] L. Spreeuwers, Fast and accurate 3D face recognition, Int. J. Comput. Vis. 93 (3) (2011) 389–414.
[2] H. Li, D. Huang, J. Morvan, Y. Wang, L. Chen, Towards 3D face recognition in the real: a registration-free approach using fine-grained matching of 3D keypoint descriptors, Int. J. Comput. Vis. 113 (2) (2015) 128–142.
[3] M. Emambakhsh, A. Evans, Nasal patches and curves for an expression-robust 3D face recognition, IEEE Trans. Pattern Anal. Mach. Intell. (2016) (1-1).
[4] G. Tam, Z. Cheng, Y. Lai, F. Langbein, Y. Liu, D. Marshall, R. Martin, X. Sun, P. Rosin, Registration of 3D point clouds and meshes: a survey from rigid to nonrigid, IEEE Trans. Vis. Comput. Graph. 19 (7) (2013) 1199–1217.
[5] H. Mohammadzade, D. Hatzinakos, Iterative closest normal point for 3D face recognition, IEEE Trans. Pattern Anal. Mach. Intell. 35 (2) (2012) 381–397.
[6] P. Besl, H. McKay, A method for registration of 3-D shapes, IEEE Trans. Pattern Anal. Mach. Intell. 14 (2) (1992) 239–256.
[7] Y.Chen, G.Medioni, Object modeling by registration of multiple range images, in: Proceedings of the IEEE International Conference on Robotics and Automation, IEEE, Sacramento, 1991, pp. 2724–2729.
[8] T. Russ, M. Koch, C. Little, A 2D range Hausdorff approach for 3D face recognition, IEEE Comput. Vis. Pattern Recognit. Workshops, IEEE, San. Diego (2005) 169–176.
[9] S. Yoshizawa, A. Belyaev, H. Seidel, Fast and robust detection of crest lines on meshes, in: Proceedings of the 2005 ACM Symposium on Solid and Physical Modeling, New York, 2005, pp. 227–232.
[10] Y. Ohtake, A. Belyaev, H. Seidel, Ridge-valley lines on meshes via implicit surface fitting, ACM Trans. Graph. 23 (3) (2004) 609–612.
[11] M. Mahoor, M. Abdel-Mottaleb, Face recognition based on 3D ridge images obtained from range data, Pattern Recognit. 45 (3) (2009) 445–451.
[12] D. Huttenlocher, G. Klanderman, W. Rucklidge, Comparing images using the Hausdorff distance, IEEE Trans. Pattern Anal. Mach. Intell. 15 (9) (1993) 850–863.
[13] C. Samir, A. Srivastava, M. Daoudi, Three-dimensional face recognition using shapes of facial curves, IEEE Trans. Pattern Anal. Mach. Intell. 28 (11) (2006) 1858–1863.
[14] S. Berretti, A. Del Bimbo, P. Pala, Sparse matching of salient facial curves for recognition of 3-D faces with missing parts, IEEE Trans. Inf. Forensics Secur. 8 (2) (2013) 374–389.
[15] S. Yoshizawa, A. Belyaev, H. Yokota, H. Seidel, Fast, robust, and faithful methods for detecting crest lines on meshes, Comput. Aided Geom. Des. 25 (8) (2008) 545–560.
[16] D. Douglas, T. Peucker, Algorithms for the reduction of the number of points required to represent a digitized line or its caricature, Cartogr.: Int. J. Geogr. Inf. Geovisualization 10 (2) (1973) 112–122.
[17] D. Sim, O. Kwon, R. Park, Object matching algorithms using robust Hausdorff distance measures, IEEE Trans. Image Process. 8 (3) (1999) 425–429.
[18] S.Rusinkiewicz, M.Levoy, Efficient variants of the ICP algorithm, in: Proceedings of the Third International Conference on 3-D Digital Imaging and Modeling, IEEE, Quebec City, 2001, pp. 145–152.
[19] A.Geiger, P.Lenz, R.Urtasun, Are we ready for autonomous driving? The KITTI vision benchmark suite, in: Proceedings of the IEEE Conference on Computer Vision and Pattern Recognition, IEEE, Providence, 2012, pp. 3354–3361.
[20] A. Moreno, A. Sánchez, GavabDB: a 3D face database, Proc. 2nd COST275 Workshop Biom. Internet, Vigo (2004) 75–80.
[21] P.Phillips, P.Flynn, T.Scruggs, K.Bowyer, J.Chang, K.Hoffman, J.Marques, J.Min, W.Worek, Overview of the face recognition grand challenge, in: Proceedings of the IEEE Conference on Computer Vision and Pattern Recognition, IEEE, San Diego, 2005, pp. 947–954.
[22] A. Mian, M. Bennamoun, R. Owens, An efficient multimodal 2D-3D hybrid approach to automatic face recognition, IEEE Trans. Pattern Anal. Mach. Intell. 29 (11) (2007) 1927–1943.
[23] F. Hajati, A. Raie, Y. Gao, 2.5D face recognition using patch geodesic moments, Pattern Recognit. 45 (3) (2012) 969–982.
[24] S.Rizvi, P.Phillips, H.Moon, The FERET verification testing protocol for face recognition algorithms, in: Proceedings of the International Conference on Automatic Face and Gesture Recognition, Nara, 1998, pp. 48–53.
[25] W. Chen, Y. Gao, Face recogntion using ensemble string matching, IEEE Trans. Image Process. 22 (12) (2013) 4798–4808.
[26] S. Islam, R. Davies, M. Bennamoun, R. Owens, A. Mian, Multibiometric human recognition using 3D ear and face features, Pattern Recognit. 46 (3) (2013) 613–627.
[27] J. Hanley, B. McNeil, The meaning and use of the area under a receiver operating characteristic (ROC) curve, Radiology 143 (1) (1982) 29–36.

Xun Yu received the M.Sc. degree in electronic engineering from Huazhong University of Science and Technology, Wuhan, China, in 2013. He is currently a PhD candidate with the School of Engineering, Griffith University, Brisbane, QLD, Australia. His research interests include 3D object recognition, face recognition, biometrics, pattern recognition, and computer vision.

Yongsheng Gao received the B.Sc. and M.Sc. degrees in electronic engineering from Zhejiang University, Hangzhou, China, in 1985 and 1988, respectively, and the Ph.D. degree in computer engineering from Nanyang Technological University, Singapore. He is currently a Professor with the School of Engineering, Griffith University, Brisbane, QLD, Australia. He had been the Leader of Biosecurity Group, Queensland Research Laboratory, National ICT Australia (ARC Centre of Excellence), a consultant of Panasonic Singapore Laboratories, and an Assistant Professor in the School of Computer Engineering, Nanyang Technological University, Singapore. His research interests include face recognition, biometrics, biosecurity, image retrieval, computer vision, pattern recognition, environmental informatics, and medical imaging.

Jun Zhou received the B.S. degree in computer science from Nanjing University of Science and Technology, Nanjing, China, in 1996, the M.S. degree in computer science from Concordia University, Montreal, Canada, in 2002, and the Ph.D. degree from the University of Alberta, Edmonton, Canada, in 2006. He is currently a Senior Lecturer in the School of Information and Communication Technology at Griffith University, Brisbane, Australia. Previously, he had been a research fellow in the Research School of Computer Science at the Australian National University, Canberra, Australia, and a researcher in the Canberra Research Laboratory, NICTA, Australia. His research interests include pattern recognition, computer vision and spectral imaging with their applications to remote sensing and environmental informatics.